Shao *et al.*
Chinese Journal of Mechanical Engineering (2022) 35:126
https://doi.org/10.1186/s10033-022-00802-4

Chinese Journal of Mechanical Engineering

ORIGINAL ARTICLE **Open Access**

Prediction and Minimization of the Heat Treatment Induced Distortion in 8620H Steel Gear: Simulation and Experimental Verification

Wen Shao*, Mohan Yi, Jinyuan Tang and Siyuan Sun

Abstract

The considerable heat treatment induced runout value in the end face of the automobile main reducer gear is always dimensionally out of tolerance. It directly affects the dimensional accuracy, the grade of carburized and hardened gears, and the post-quenching manufacturing costs. In this study, three dimensional numerical models were developed to simulate the carburizing-quenching process of gear based on the multi-field coupling theory using DEFORM software. The results indicated that the ununiform cooling rate of the gear caused by the asymmetry of the web structure would result in the ununiform distribution of martensite, leading to the large runout value at the end face of the gear. Therefore, a novel method was proposed to minimize the heat treatment induced runout value. It was found that the heat treatment induced runout value could be effectively controlled by the addition of a compensation ring and the support of a rod structure. Further experiments showed that the average runout value of the gear end face before and after the proposed heat treatment method were about 0.023 mm and 0.059 mm respectively, which was in good agreement with the simulated results. The novel approach proposed in this study led to a reduction of the gear runout value by 70.0%–76.9% compared to that of the original heat treatment process, which may serve as a practical and economical way to predict and minimize the heat treatment induced distortion in drive gear.

Keywords: Distortion, Carburizing-quenching, Numerical simulation, Heat treatment, 8620H steel gear

1 Introduction

As the core components for the transmission of movement and torque, gear drives are progressively being used in aircraft, high speed rail, automobile, and robot industries [1, 2]. The increasing demand of gears drive in these fields leads to a much more rigorous requirement for the surface integrity [3, 4], geometric and physical performances [5, 6], and fatigue life [7] of it. As a vital process in gear manufacturing, heat treatment exerts an enormous function on the enhancement of gear quality such as strength, surface hardness, wear and fatigue behaviors [8, 9]. However, excessive and uncontrolled distortion may inevitably occur due to the comprehensive impacts of the materials, structures, quenching medias, thermal stresses and phase transformations during the heat treatment [10, 11]. Therefore, it is of great importance to predict and minimize the heat treatment induced distortion as it directly affects the dimensional accuracy, the grade of carburized and hardened gears, and the post-quenching manufacturing costs.

Apart from the improper selection of material such as chemical composition, structure and geometry, the heat treatment characteristics (furnace type, detailed position inside the chamber, cooling uniformity, treatment gases and cooling medium) play an essential role in the final detail distortions in the process of toothed gears manufacturing [12–14]. There are several popular methods such as gas quenching [12] and cryogenic treatment [15] to minimize the distortion in industry.

*Correspondence: shaowen_2013@163.com; wen.shao@csu.edu.cn

State Key Laboratory of High Performance Complex Manufacturing, College of Mechanical and Electrical Engineering, Central South University, Changsha 410083, China

Investigations were conducted to predict and optimize the quenching process by the change of the heat transfer coefficient (HTC) [16, 17]. Lee et al. [18] investigated the relationship between phase transformation kinetics and distortion and established the martensitic dynamic equation. Sugianto et al. [19] studied the effect of phase transformation induced plasticity on the tooth distortion of heat-treated helical gears. Nallathambi et al. [20] performed the sensitivity analyses of material properties on distortion and residual stresses during metal quenching processes. The material properties such as metallergical properties, yield stress, and bulk modulus were found to have positive effect on the simultaneous distortion and residual stresses under the same cooling condition. Pang et al. [21] optimized the gear shaft structure to improve the gear shaft quality, reduce the energy waste and lower the corresponding cost during the quenching process.

Most of the above stated researches have been focused on the reduction or optimization of the heat treatment induced distortion and residual stress by the change of cooling rate through the proper selection of quenching medium and temperature. Despite of the efforts of these earlier studies, difficulty and limitation still exist for the prediction and minimization of the heat treatment induced distortion of the automobile main reducer gear in the present study. For example, it is difficult to apply gas quenching for gears with large size and hard to solve the inhomogeneous cooling rate caused by asymmetric gear structure. Moreover, there is little space for the adjustment of the HTC in traditional liquid quenching process. Unlike experimental investigations, numerical or theoretical methods are capable of yielding multiple results within a short period, optimizing comprehensive manufacturing processes with sufficient data sets, and sometimes offering useful visualization of various stages of machining processes [22–25]. In this study, three dimensional numerical models will be developed to simulate the carburizing-quenching process and determine the cause for severe deformation of the gear. Then, an innovative optimization method is proposed to minimize the heat treatment induced distortion. Finally, heat treatment experiments are further conducted to verify the validity of the proposed approach.

2 Mathematical Formulation

2.1 Heat Transfer

The basic heat transfer law of temperature field is Fourier's law. According to the conservation law of energy, the three-dimensional heat transfer differential equation is expressed as [26]:

$$\rho c_p \frac{\partial T}{\partial \tau} = \lambda \frac{\partial^2 T}{\partial x_i^2} + \sigma_{ij}\dot{\varepsilon}_{ij}^p - \sum \rho_I l_I \dot{\zeta}_I, \tag{1}$$

where T is the temperature, ρ is the density, c_p is the specific heat, λ is the heat conduction coefficient, l_I is the latent heat due to phase transformation. The heat transfer between the sample and the medium belongs to the third type of boundary condition.

$$-\lambda \frac{\partial T}{\partial n}\bigg| = H_k\left(T - T_f\right), \tag{2}$$

where H_k is the coefficient of heat transfer, T is the surface temperature, T_f is the medium temperature.

2.2 Diffusion Equation

The actual process of carburizing and diffusion is an unsteady state and the basic governing equation is known as Fick's second law:

$$\frac{\partial C}{\partial \tau} = \frac{\partial}{\partial x_i}\left(D\frac{\partial C}{\partial x_i}\right), \tag{3}$$

where C is the carbon content, τ is the time, x_i is the position direction, D is the diffusion coefficient of carbon in austenite, which could be determined by the following empirical equation [27]:

$$\begin{aligned} D(T,C) = &\begin{pmatrix} 0.146 - 0.036(1 - 1.075Cr) - 0.0315Mn + 0.0509Si \\ -0.0085Ni + 0.3031Mo - 0.052Al \end{pmatrix} \\ &\cdot \exp\left(-\frac{\begin{matrix} 144300 - 15000C + 370C^2 - 4366.3Mn + 4050.7Si \\ -1240.7Ni + 7726Cr + 12126.6Mo - 6788.6Al \end{matrix}}{R_J T}\right), \end{aligned} \tag{4}$$

where R_J is the gas constant (8.314 J/mol/K). In most cases the boundary condition for carbon diffusion equation is calculated as:

$$-D\frac{\partial C}{\partial x_i} = \beta\left(C_g - C_s\right), \tag{5}$$

where C_g is the practical carbon content, C_s is the carbon content in the surface, β is the coefficient of carbon mass transferred from the atmosphere to the surface, which is given by

$$\beta = \beta_0 \exp\left(-\frac{E}{RT}\right), \tag{6}$$

where β_0 is constant (0.00347 mm/s), E is the activation energy (34 kJ/mol).

2.3 Phase Transformation Kinetics

In the carburizing-quenching process, the C content exerts an enormous function on the phase transformation temperature. The specific value of the starting temperature of martensite transformation M_s can be calculated from the following empirical formulation [18]:

$$\begin{aligned} M_s\left(^\circ\mathrm{C}\right) = 402 - 797C + 14.4Mn + 15.3Si \\ - 31.1Ni + 345.6Cr \\ + 434.6Mo + (59.6C + 3.8Ni \\ -41Cr - 53.8Mo) \cdot G. \end{aligned} \tag{7}$$

Therefore, both the weight percent of each element including C, Mn, Si, Ni, Cr, Mo contents and ASTM austenite grain size number G affect the M_s. The M_s temperature will decrease with the increase of C content.

Solid-state phase transition can generally be divided into diffusion and non-diffusion phase transitions according to atomic migration in the phase transition process. The transformation from austenite to other tissues, such as ferrite, pearlite and bainite, is a diffusion transformation. The phase change from austentite to martensite belongs to non-diffusion phase transition. The initial tissues transformed into austenite can be obtained from the following diffusion equation:

$$\xi_A = 1 - \exp\left\{A\left[\frac{T - A_{c1}}{A_{c3} - A_{c1}}\right]^D\right\}, \tag{8}$$

where ξ_A is the volume fraction of austenite, A_{c1} is the starting temperature of phase transition, A_{c3} is the end temperature of phase transition, A and D are material constants (−4 and 2).

The diffusion phase transformation is calculated by Johnson-Mehl equation:

$$f(t) = 1 - \exp\left(-Kt^n\right), \tag{9}$$

where K and n are the material constants. K is determined by the temperature, the composition of the original phase, and the grain size, and n is determined by the phase change type.

The martensitic transformation is predicted by K-M equation [28]:

$$\xi_M = 1 - \exp\left[-\alpha(M_s - T)\right], \tag{10}$$

where M_s is the starting temperature of martensite transformation, α is a constant (1.1×10^{-2} K^{-1}).

2.4 Stress-Strain Relationships

In the heat treatment simulation, the calculation of the plastic flow stress depends on the flow stress curve of each phase which can be expressed as a function of strain, strain rate and temperature [29–31]:

$$\overline{\sigma}=\overline{\sigma}(\varepsilon, \dot{\varepsilon}, T). \tag{11}$$

The total strain rate is defined as:

$$\dot{\varepsilon}_{ij} = \dot{\varepsilon}_{ij}^{t} + \dot{\varepsilon}_{ij}^{e} + \dot{\varepsilon}_{ij}^{p} + \dot{\varepsilon}_{ij}^{tr} + \dot{\varepsilon}_{ij}^{tp}, \tag{12}$$

where $\dot{\varepsilon}_{ij}^{t}$, $\dot{\varepsilon}_{ij}^{e}$, $\dot{\varepsilon}_{ij}^{p}$, $\dot{\varepsilon}_{ij}^{tr}$ and $\dot{\varepsilon}_{ij}^{tp}$ are the thermal, elastic, plastic, phase transformation and phase transformation plasticity strain rates.

The thermal strain rate is related to the instantaneous thermal expansion coefficient α and the temperature change $\Delta\dot{T}$:

$$\dot{\varepsilon}_{ij}^{t} = \alpha\dot{T}\delta_{ij}. \tag{13}$$

The elastic strain rate is expressed as:

$$\dot{\varepsilon}_{ij}^{e} = \frac{1+\upsilon}{E}\dot{\sigma}_{ij} - \frac{\upsilon}{E}\dot{\sigma}_{kk}\delta_{ij}, \tag{14}$$

where E is the Young's modulus, υ is the Poisson's ratio.

The plastic strain rate is given by:

$$\dot{\varepsilon}_{ij}^{p} = \hat{G}\left(\frac{\partial F}{\partial \sigma_{kl}}\dot{\sigma}_{kl} + \frac{\partial F}{\partial T}\dot{T} + \sum\frac{\partial F}{\partial \xi_{ij}}\dot{\xi}_{ij} + \frac{\partial F}{\partial c}\dot{C}\right)\frac{\partial F}{\partial \sigma_{ij}}, \tag{15}$$

where F is the total yield function as mixture phase, σ_{ij} is the flow stress.

The phase transformation strain rate is derived from:

$$\dot{\varepsilon}_{ij}^{tr} = \sum\nolimits_{I=1}^{N}\beta_{IJ}\dot{\xi}_{IJ}\delta_{ij}, \tag{16}$$

where β_{IJ} is the coefficient of the phase transformation in fractional length change due to phase change from I to J instantaneously. $\dot{\xi}_{IJ}$ is the volume fraction rate of the phase transformation which is the time differentiation of the transformation volume fraction from phase I to J.

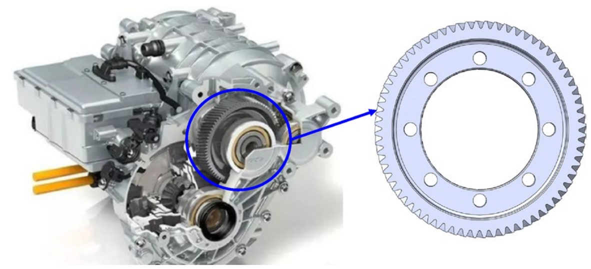

Figure 1 Configuration of the 8620H gear

Table 1 Composition of the 8620H material

Material type	C	Si	Mn	Cr	Mo
8620H	0.17	0.21	0.84	0.57	0.20
Material type	Ni	Al	P	S	Cu
8620H	0.45	0.02	0.01	0.02	0.1

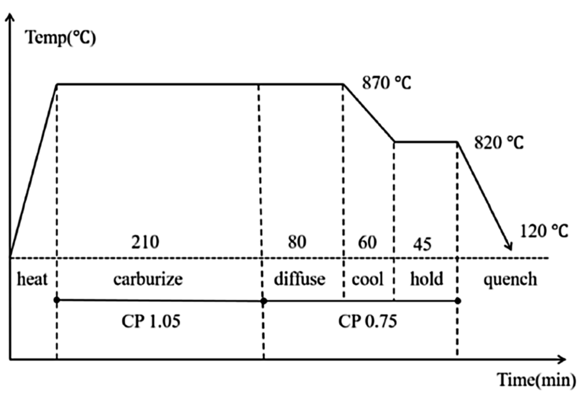

Figure 2 The curve of gear heat treatment process

The phase transformation plasticity strain rate is expressed as:

$$\dot{\varepsilon}_{ij}^{tp} = 1.5\sum\nolimits_{I=1}^{N} K_{IJ} h\left(\dot{\xi}_{IJ}\right)\xi_{IJ} S_{ij}, \tag{17}$$

$$h\left(\dot{\xi}_{IJ}\right) = 2\left(1 - \xi_{IJ}\right), \tag{18}$$

where K_{IJ} is the coefficient of transformation plasticity for diffusionless martensitic or diffusion bainitic transformation. $h(\dot{\xi_{IJ}})$ is the contribution from transformation progress to the transformation plasticity strain. ξ_{IJ} is the rate of phase transformation and S_{ij} is the shear stress.

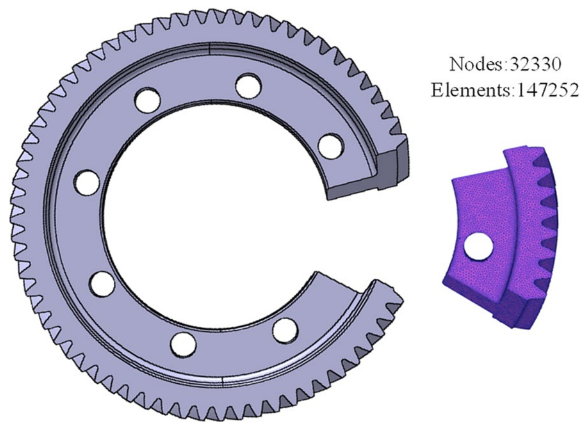

Figure 3 3D finite element model of the 8620H gear with 8 teeth

Table 2 Material properties of 8620H gear

T (℃)	*cp* (J/(kg·℃))	*λ* (W/(m·℃))	*ρ* (kg/m^3)	*μ*	*E* (GPa)
25	0.45536	69.20361	7840.76	0.28910	211.9596
100	0.48450	64.00208	7824.46	0.29192	208.6537
200	0.52816	56.27197	7796.21	0.29551	202.6909
300	0.58864	48.92402	7762.95	0.29936	194.6552
400	0.62724	43.19080	7728.25	0.30326	184.5198
500	0.71848	38.59421	7691.57	0.30718	172.5068
600	0.80211	34.91778	7653.60	0.31109	159.0304
700	0.96772	32.34905	7615.17	0.31528	144.3853
800	1.01789	26.85362	7642.12	0.33707	127.6197
900	0.60977	27.50721	7599.67	0.34546	117.4178
1000	0.62525	28.71413	7545.75	0.35137	107.4592
1100	0.64081	29.92103	7492.36	0.35727	97.36888
1200	0.65653	31.12793	7439.47	0.36318	87.14697

3 Simulation Details

The investigated gear in this study is the driven gear of the automotive main reducer, which is dimensionally out of tolerance with a runout value of 0.10–0.13 mm after carburizing-quenching. It has a modulus of 2.35, teeth number of 68 and pressure angle of 20°, as shown in Figure 1. The gear material is 8620H steel. The composition of it is listed in Table 1. The detailed heat treatment process is shown in Figure 2 with a carburizing temperature of 870 °C, quenching start temperature of 820 °C and oil temperature of 120 °C. According to the principle of symmetry, 8 teeth of the gear were taken for the simulation tests. The 3D FEM model was created with 147252 tetrahedral elements and 32330 nodes (Figure 3). All the elements and nodes were set to be elasto-plastic using the Newton-Raphson iterative method.

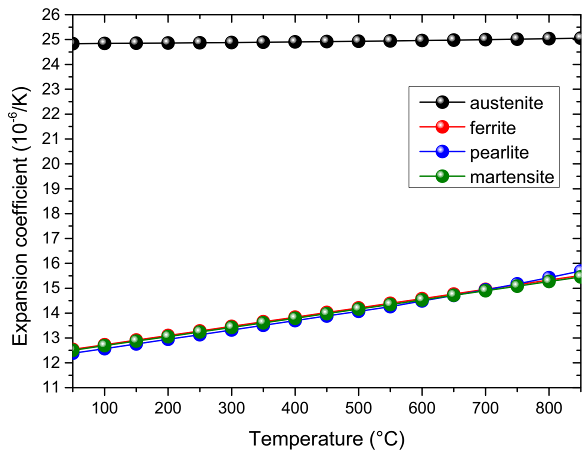

Figure 4 Expansion coefficients of 8620H gear

3.1 Material Properties

The mechanical and thermal properties of the 8620H material under low temperature were obtained from Ref. [32]. While the mechanical and thermal properties of it under high temperature were established by Jmatpro software. The detailed parameters are shown in Table 2 and Figure 4.

3.2 Heat Transfer Coefficient

Accurate heat transfer coefficient in oil quenching is the basis for the simulation of the microstructure evolution during quenching. The heat transfer coefficients of various common steels in different quenching media, measured by Wang [32], were used as a reference in this study. The heat transfer coefficients do not change obviously during heating and carburizing processes, thus

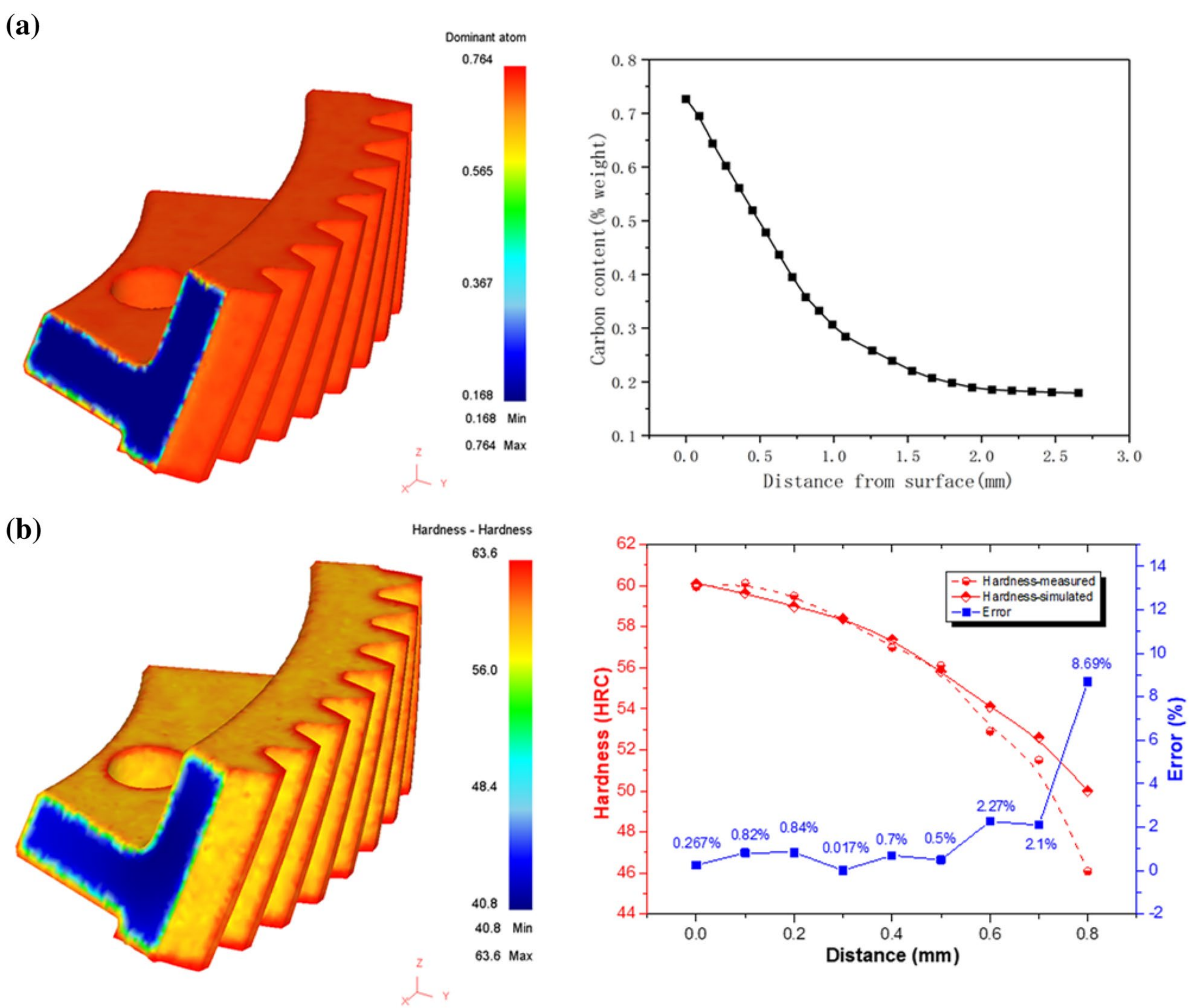

Figure 5 Carbon content (**a**) and hardness distribution (**b**) of the carburized-quenched gear

could be set as constants, i.e., 0.1 and 0.05 N/s/mm/°C, respectively.

4 Results

4.1 Carbon Content and Hardness Distribution

As shown in Figure 5(a), the carbon content of the carburized 8620H gear decreased continuously from 0.72% at the surface to 0.17% in the core. As depicted in Figure 5(b), the associated hardness of the gear changed from 60 HRC to 40 HRC, which was in extremely good agreement with the measured hardness under the same heat treatment conditions. The effective hardened layer with hardness higher than 52 HRC was about 0.6 mm deep. Most of the errors between the simulated and measured hardness under the gear surface were within 1%. The average and maximum error of the simulated hardness were found to be 1.8% and 8.69% respectively.

4.2 Metallographic Transformation

The metallographic transformation will occur when the temperature increase or decrease to a phase transition temperature. Figure 6 illustrates phase transformation of the 8620H gear during the carburizing and quenching process. In the initial heating stage, the gear is austenitized and the metallographic structure of whole gear is austenite. As discussed previously, the M_s temperature will decrease with the increase of carbon content. The carbon content of the carburized 8620H gear at the gear surface (0.72%) was much higher than that in the core (0.17%), which would lead to a much higher M_s point in the core of the gear. Therefore, the martensite transformation took place in the core first as the quenching starts. Then, the martensite transformation gradually diffused to the surface of the gear as the quenching continues. It was evident that the volume fraction of the martensite in the core was much higher than that at the surface of the teeth and gear wed.

4.3 Distortion Analysis

Though heat treatment has great effect on the enhancement of gear quality such as strength, surface hardness, wear and fatigue behaviors, excessive and uncontrolled distortion may inevitably be induced. As shown in Figure 7, it is evident that the distortion at the end face of the gear is ununiform and appears gradient distribution, i.e., expanded at the tooth surface while contracted

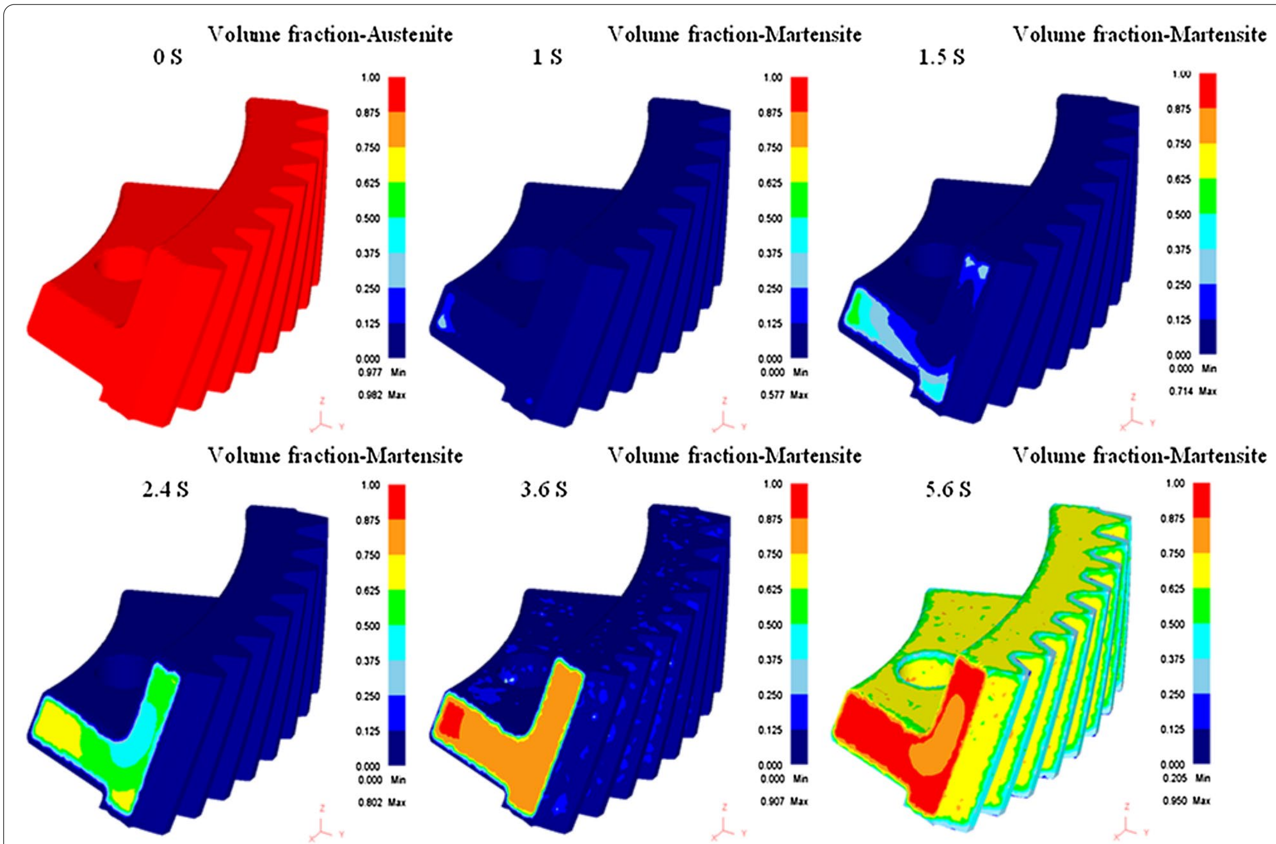

Figure 6 The metallographic transformation during the quenching process

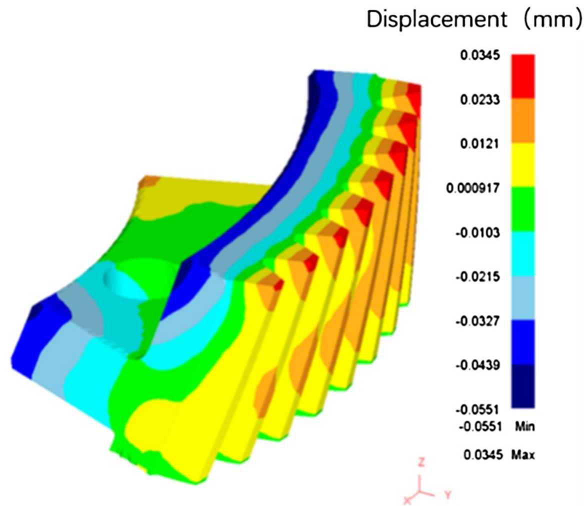

Figure 7 Numerical simulation of the heat treatment induced distortion

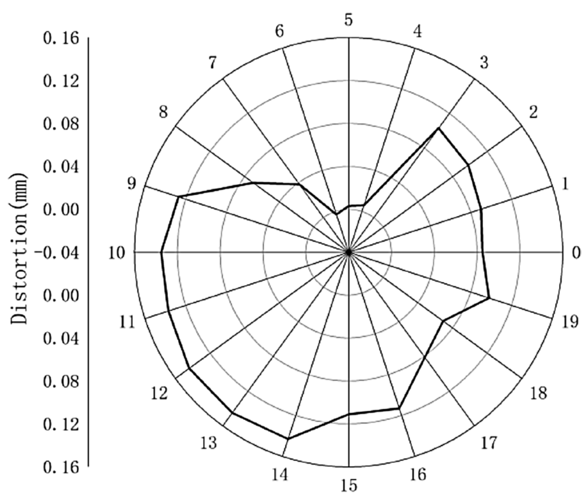

Figure 8 Experimental verification of the heat treatment induced distortion

at the end surface. A maximum expansion deformation of 0.035 mm (in red) was found at tooth surface while a contraction of 0.055 mm was observed at the end surface of the gear (in blue). The runout value at the end face of the tooth is around 0.09 mm. As shown in Figure 8, the actual distortion measured by a trilinear coordinates measuring instrument showed the runout value at the end face of the gear varied from 0.10 mm to 0.13 mm, which was close to the simulated distortion results. The numerical and experimental results indicated that FEM modeling was capable of predicting the deformation and microstructure evolution during heat treatment process, therefore adopt in this study for the minimization of the associated distortion.

4.4 Temperature Changes

In order to identify the causes of gear deformation, the temperature changes and distribution of the gear during quenching were further extracted and analyzed in this study. The temperature changes and distribution of the gear shown in Figure 9 indicated that there was an obvious temperature difference between the surface of the gear and the core as soon as the quenching process starts. The cooling rate of the gear surface was faster than that of the core and the cooling rate of the gear web was faster than that of the teeth. The temperature of the entire gear tended to be uniform and the temperature difference between the gear surface and the core vanished as the gear was quenched for 25.5 s.

The temperature variations of the gear surface and the core during quenching were shown in Figure 10. It was obvious that the cooling rate of the gear surface was much faster than that of the core in the first 15 s of the quenching process. Beyond this point, there was only a slight decrease of temperature for both of them and the cooling rate of the gear tended to be stabilized. The maximum temperature difference between the gear surface and the core was obtained as 280 °C.

5 Discussion

The simulation results indicated that the non-uniform cooling rate and large temperature gradient of the gear caused by the asymmetry of the web structure might be the determinant of severe deformation of the gear. If the cooling situation of the gear is well controlled during the quenching process, better uniformity of the gear can be obtained to reduce the heat treatment induced distortion. Therefore, a novel method was further proposed accordingly to minimize the heat treatment induced distortion.

5.1 Details of the Distortion Minimization Method

The novel measure was designed through the addition of a compensation ring and the support of a rod structure. As shown in Figure 11, the compensation ring also made of 8620H steel which was defined as a rigid body during simulation. The support rod was specifically developed according to the gear size. The assembly drawing of the whole structure was shown in Figure 12.

5.2 Temperature Changes

The comparison of the temperature changes for both the gear surface and the core during quenching between the original process and the new measure are shown in

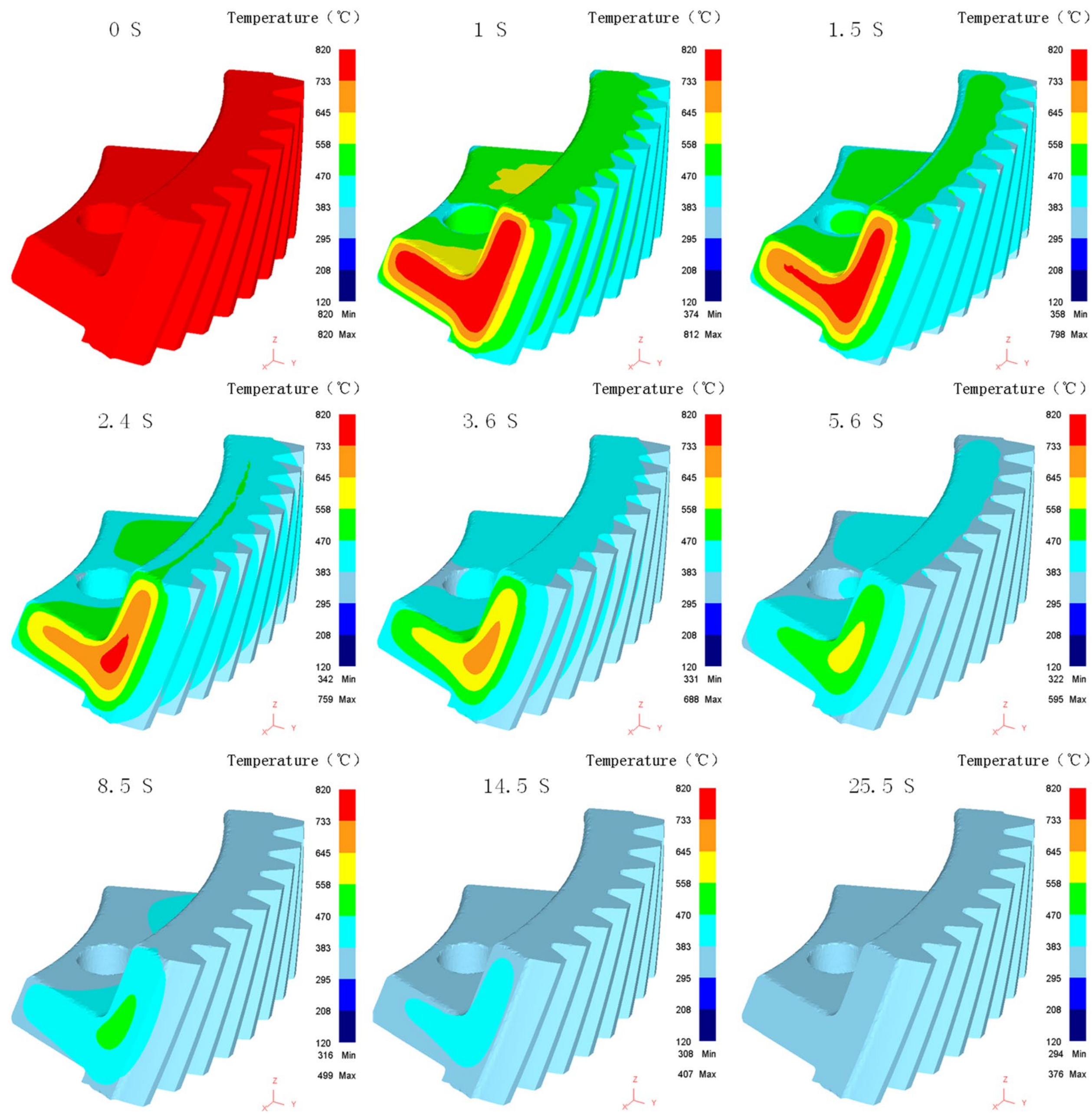

Figure 9 Temperature distribution during the quenching process

Figure 13. As shown in Figure 13, the trend and magnitude of the temperatures of the gear surface and the core for the new measure are, in general, consistent with those of the original quenching and cooling process. In the whole cooling process, the temperature difference between the gear surface and the core of new measure were smaller than that of the original process. The maximum temperature difference reduced from 280 ℃ to 210 ℃.

5.3 Phase Fractions and Distribution

The quantitative phase fractions of martensite and ferrite developed on the gear surface and in the core for all the original process and the new measure are compared and presented in Figure 14. For the original process, the fractions of martensite and ferrite developed on the gear surface and in the core were 91%, 2% and 88%, 8% respectively. For the new measure, the martensite fractions developed on the gear surface and in the core increased

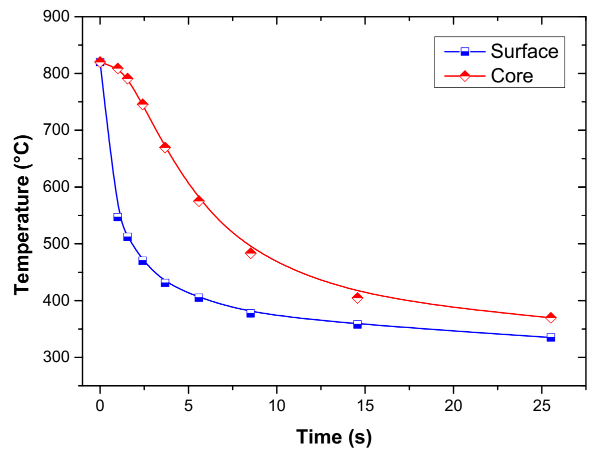

Figure 10 Curves of temperature changes during gear quenching

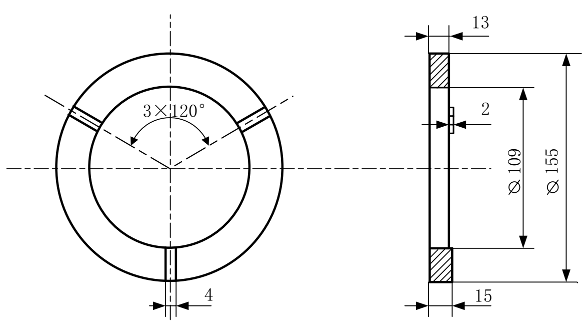

Figure 11 Configuration and detailed dimension of the compensation ring

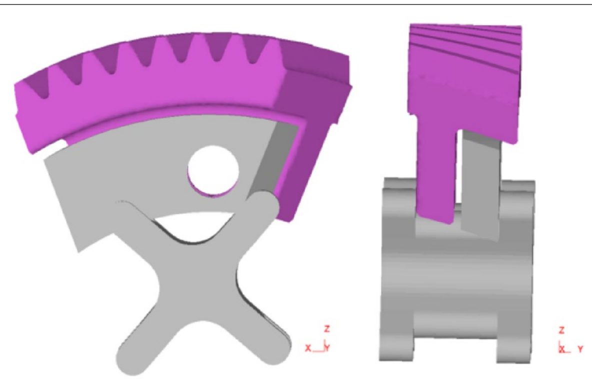

Figure 12 The assembly drawing of the instrumented gear

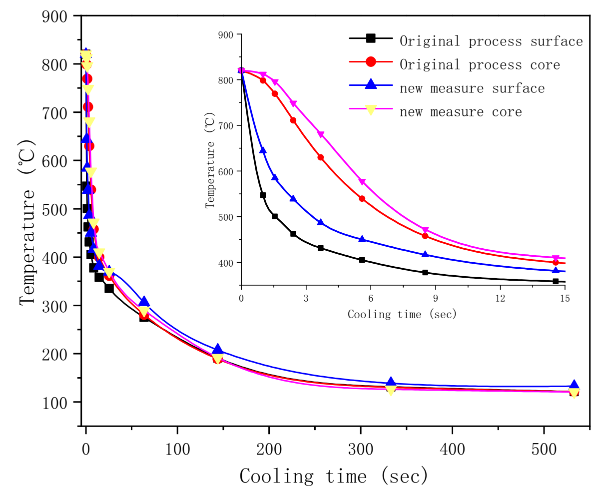

Figure 13 Comparison of the temperature changes for the gear surface and the core during quenching between the original process and the new measure

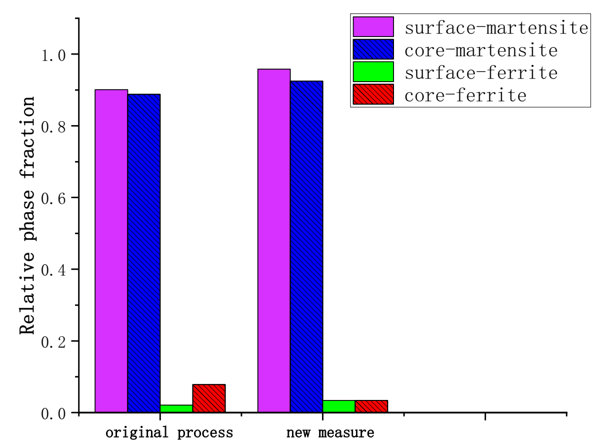

Figure 14 Comparison of phase fractions of the gear for the original method and new method

to 96% and 92%. The ferrite fraction on the gear surface increased to 3%, while this phase fraction in the core decreased to 3%.

The detailed distribution of martensite for the new method and the original process are shown in Figure 15. It can be seen from the figure that the distribution of martensite on the surface developed for the original process was discrepant at different regions. While the martensite distribution both on the gear surface and in the core for the new measure were fairly uniform.

5.4 Distortion Analysis of the New Measure

The distortion of the new measures is shown in Figure 16. As can be seen from Figure 16, the distortion at the end face of gear and tooth for the last approach is extremely uniform with a magnitude of around 0.13 mm. The runout value at the end face of the tooth is around 0.02. The reason accounting for the relatively small runout

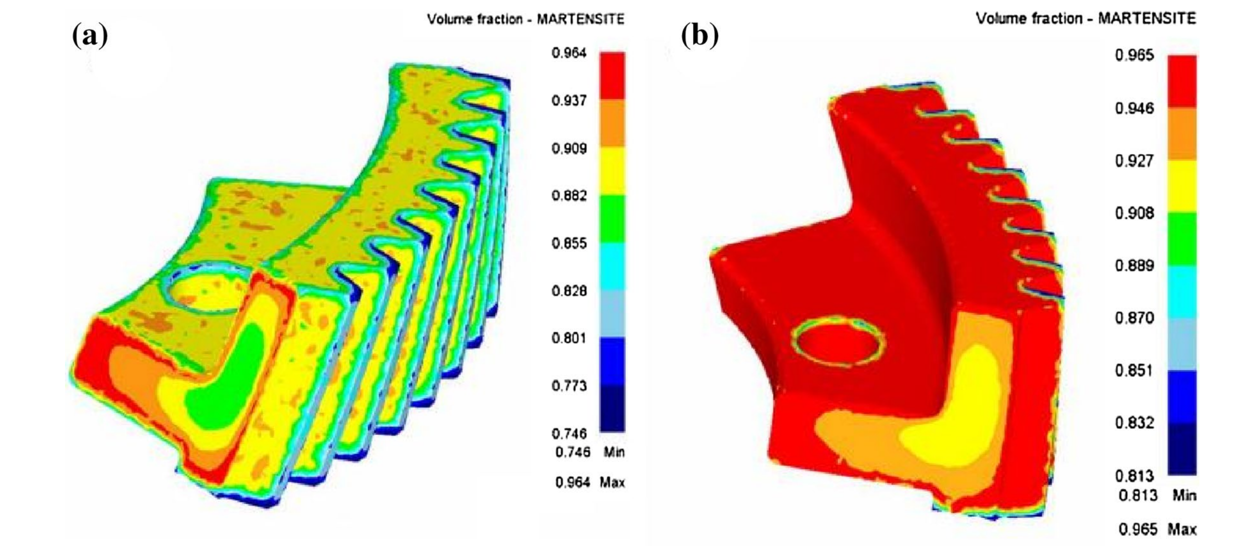

Figure 15 The detailed distribution of martensite of the gear for **a** the original method and **b** the new method

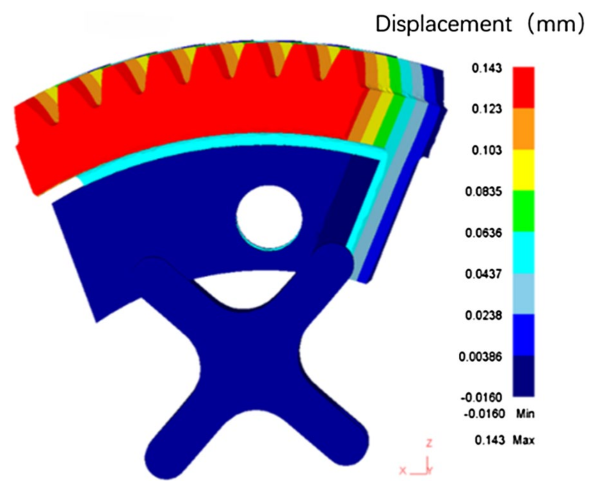

Figure 16 Heat treatment induced distortion of the gear for the new method

Figure 17 Gears assembly diagram

value at the end face of the gear might be the corresponding uniform martensite distribution.

5.5 Experimental Verification

Further heat treatment experiments were conducted to verify the validity of the numerical results. The total number of gear assemblies was 20 (Figure 17).

The experimental results are shown in Table 3 and Figure 18. The distortion at the end face was found to be significantly improved compared to that of the original heat treatment process. The average runout value at the end face of the gear before and after heat treatment were 0.023 mm and 0.052 mm respectively. The average difference value was 0.029 mm, which was in good agreement with the simulated results.

The novel approach proposed in this study led to a reduction of gear runout value by 70.0%–76.9% compared with 0.10 mm to 0.13 mm of the original process, which may serve as a practical and economical way to predict and minimize the heat treatment induced distortion in drive gear.

6 Conclusions

The heat treatment induced distortion of 8620H steel gear were predicted and a novel approach was proposed to minimize it. The main conclusions drawn from this study can be summarized as follows.

(1) Three dimensional numerical models were successfully developed to simulate the carburizing-

Table 3 The measured distortion results of the gear for the new method

Gear No.	Runout value before heat treatment (mm)	Runout value after heat treatment (mm)	Difference value
1	0.020	0.050	0.030
2	0.020	0.050	0.030
3	0.020	0.080	0.060
4	0.040	0.040	0.000
5	0.030	0.070	0.040
6	0.040	0.050	0.010
7	0.030	0.080	0.050
8	0.010	0.080	0.070
9	0.035	0.070	0.035
10	0.020	0.030	0.010
11	0.020	0.040	0.020
12	0.020	0.060	0.040
13	0.025	0.040	0.015
14	0.020	0.060	0.040
15	0.030	0.050	0.020
16	0.010	0.040	0.030
17	0.010	0.030	0.020
18	0.010	0.030	0.020
19	0.020	0.040	0.020
20	0.020	0.050	0.030
Average	0.023	0.052	0.029

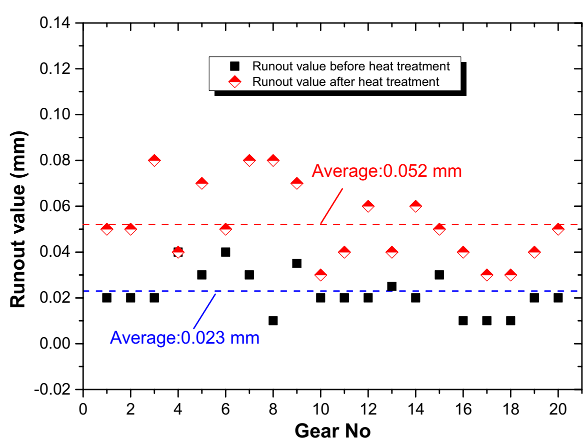

Figure 18 Runout value at the end face of the gear before and after heat treatment

quenching process of gear based on the multi-field coupling theory using DEFORM software. The predicted distortion and hardness distribution at the end face of the gear were in extremely good agreement with those of the measured ones.

(2) The reason accounting for the relatively small runout value at the end face of the gear for the proposed method might be the corresponding uniform martensite distribution. The simulation results indicated that the ununiform cooling rate and large temperature gradient of the gear caused by the asymmetry of the web structure would result in the ununiform distribution of martensite. If the cooling situation of the gear is well controlled during the quenching process, better uniformity of the martensite distribution of the gear can be obtained to reduce the heat treatment induced runout value.

(3) A novel measure was proposed to minimize the heat treatment induced distortion. It was found that the heat treatment induced distortion could be effectively controlled by the addition of a compensation ring and the support of a rod structure. Further experiments showed that the average runout value of the gear end face before and after the proposed heat treatment method were about 0.023 mm and 0.059 mm respectively, which correlated well with the simulated results. The novel approach proposed in this study led to a reduction of the gear distortion by 70.0%–76.9% compared to that of the original heat treatment process, which may serve as a practical and economical way to predict and minimize the heat treatment induced distortion in drive gear.

Acknowledgements
Not applicable.

Authors' Contributions
WS and MY wrote the manuscript; WS guided the numerical simulations and experiments; MY and SS assisted with the numerical simulation and experimental analyses; JT and SS reviewed and edited the manuscript. All authors read and approved the final manuscript.

Authors' Information
Wen Shao born in 1987, is an associate professor at *State Key Laboratory of High Performance Complex Manufacturing, College of Mechanical and Electrical Engineering, Central South University, China*. He received his Ph.D. degree from *The University of Queensland, Australia*, in 2016. His main research is focused on ultra-precision machining and anti-fatigue manufacturing of complex surface components. Tel: +86-185-08485061
Mohan Yi, born in 1999, is a master candidate at *College of Mechanical and Electrical Engineering, Central South University, China*. His research is focused on heat treatment and machining of gears.
Jinyuan Tang, born in 1962, is a professor and the Vice Director of *State Key Laboratory of High Performance Complex Manufacturing, College of Mechanical and Electrical Engineering, Central South University, China*. He has been doing both fundamental studies and application researches in the areas of ultra-precision machining, high performance design and manufacture of complex surface components including cam, face, spiral bevel, hypoid and cylindrical gears.
Siyuan Sun, born in 1994, is a master candidate at *College of Mechanical and Electrical Engineering, Central South University, China*. His research is focused on heat treatment of gears.

Funding

Supported by National Key R&D Program of China (Grant No. 2019YFB2004700), State Key Laboratory of High Performance Complex Manufacturing of China (Grant No. ZZYJKT2019-08), and China Postdoctoral International Exchange Program (Grant No. 140050004).

Competing Interests

The authors declare no competing financial interests.

Received: 16 September 2022 Revised: 16 September 2022 Accepted: 19 September 2022
Published online: 20 October 2022

References

[1] H Ding, J Y Tang, W Shao, et al. Optimal modification of tooth flank form error considering measurement and compensation of cutter geometric errors for spiral bevel and hypoid gears. *Mechanism and Machine Theory*, 2017, 118: 14-31.
[2] W Shao, H Ding, J Y Tang. Data-driven operation and compensation approaches to tooth flank form error measurement for spiral bevel and hypoid gears. *Measurement*, 2018, 122: 347-357.
[3] R Rego, C Löpenhaus, J Gomes, et al. Residual stress interaction on gear manufacturing. *Journal of Materials Processing Technology*, 2018, 252: 249-258.
[4] W H Zhou, J Y Tang, H F Chen, et al. Modeling of tooth surface topography in continuous generating grinding based on measured topography of grinding worm. *Mechanism and Machine Theory*, 2019, 131: 189-203.
[5] H Ding, J Y Tang, W Shao, et al. An innovative determination approach to tooth compliance for spiral bevel and hypoid gears by using double-curved shell model and Rayleigh–Ritz approach. *Mechanism and Machine Theory*, 2018, 130: 27-46.
[6] W H Zhou, J Y Tang, H F Chen, et al. A comprehensive investigation of plowing and grain-workpiece micro interactions on 3D ground surface topography. *International Journal of Mechanical Sciences*, 2018, 144: 639-653.
[7] H Ding, H P Li, W Shao, et al. Prediction and control for local bearing contact-based collaborative grinding of non-orthogonal aerospace spiral bevel gears. *Mechanical Systems and Signal Processing*, 2021, 160: 107841.
[8] D W Kim, H H Cho, W B Lee, et al. A finite element simulation for carburizing heat treatment of automotive gear ring incorporating transformation plasticity. *Materials & Design*, 2016, 99: 243-253.
[9] W Wang, H J Liu, C C Zhu, et al. Effect of the residual stress on contact fatigue of a wind turbine carburized gear with multiaxial fatigue criteria. *International Journal of Mechanical Sciences*, 2019, 151: 263-273.
[10] Y Bouissa, N Bohlooli, D Shahriari, et al. FEM modeling and experimental validation of quench-induced distortions of large size steel forgings. *Journal of Manufacturing Processes*, 2020, 58: 592-605.
[11] R D López-García, F A García-Pastor, A Maldonado-Reyes, et al. Analysis of the effect of immersion rate on the distortion and residual stresses in quenched SAE 5160 steel using FEM. *Journal of Materials Research and Technology*, 2019, 8(6): 5557-5571.
[12] R Atraszkiewicz, B Januszewicz, Ł Kaczmarek, et al. High pressure gas quenching: Distortion analysis in gears after heat treatment. *Materials Science and Engineering: A*, 2012, 558: 550-557.
[13] H Ding, H P Li, R Huang, et al. Adaptive data-driven prediction and optimization of tooth flank heat treatment deformation for aerospace spiral bevel gears by considering carburizing-meshing coupling effect. *International Journal of Heat and Mass Transfer*, 2021, 174: 121301.
[14] V García Navas, O Gonzalo, I Quintana, et al. Residual stresses and structural changes generated at different steps of the manufacturing of gears: Effect of banded structures. *Materials Science and Engineering: A*, 2011, 528(15): 5146-5157.
[15] T Sonar, S Lomte, C Gogte, et al. Minimization of distortion in heat treated AISI D2 tool steel: Mechanism and distortion analysis. *Procedia Manufacturing*, 2018, 20: 113-118.
[16] Z Li, R V Grandhi, R Srinivasan. Distortion minimization during gas quenching process. *Journal of Materials Processing Technology*, 2006, 172(2): 249-257.
[17] A Sugianto, M Narazaki, K Michiharu, et al. Numerical simulation and experimental verification of carburizing-quenching process of SCr420H steel helical gear. *Journal of Materials Processing Technology*, 2009, 209(7): 3597-3609.
[18] S J Lee, Y K Lee. Finite element simulation of quench distortion in a low-alloy steel incorporating transformation kinetics. *Acta Materialia*, 2008, 56(7): 1482-1490.
[19] A Sugianto, M Narazaki, M Kogawara, et al. The effect of transformation plasticity on prediction of tooth distortion of heat-treated helical gear. *Materials Science Forum*, 2007, 561-565: 1853-1856.
[20] A K Nallathambi, Y Kaymak, E Specht, et al. Sensitivity of material properties on distortion and residual stresses during metal quenching processes. *Journal of Materials Processing Technology*, 2010, 210(2): 204-211.
[21] Z Pang, S Yu, J Xu. Study of effect of quenching deformation influenced by 17CrNiMo6 gear shaft of carburization. *Physics Procedia*, 2013, 50: 103-112.
[22] D R Liao, W Shao, J Y Tang, et al. An improved rough surface modeling method based on linear transformation technique. *Tribology International*, 2018, 119: 786-794.
[23] D R Liao, W Shao, J Y Tang, et al. Numerical generation of grinding wheel surfaces based on time series method. *The International Journal of Advanced Manufacturing Technology*, 2018, 94(1): 561-569.
[24] S Y Sun, J Y Tang, W Shao, et al. Research on the matching relationship between ultrasonic-assisted grinding parameters and workpiece surface roughness. *The International Journal of Advanced Manufacturing Technology*, 2019, 102(1): 487-496.
[25] W H Zhou, J Y Tang, H F Chen, et al. A comprehensive investigation of surface generation and material removal characteristics in ultrasonic vibration assisted grinding. *International Journal of Mechanical Sciences*, 2019, 156: 14-30.
[26] T Inoue. Mechanics and characteristics of transformation plasticity and metallo-thermo-mechanical process simulation. *Procedia Engineering*, 2011, 10(7): 3793-3798.
[27] R C Goertz, R C Thompson. Electronically controlled manipulators. *Nucleonics*, 1954, 12(11): 46-47.
[28] S H Kang, Y J Im. Three-dimensional thermo-elastic–plastic finite element modeling of quenching process of plain-carbon steel in couple with phase transformation. *International Journal of Mechanical Sciences*, 2007, 49(4): 423-439.
[29] B L Ferguson, Z Li, A M Freborg. Modeling heat treatment of steel parts. *Computational Materials Science*, 2005, 34(3): 274-281.
[30] C Şimşir, C H Gür. 3D FEM simulation of steel quenching and investigation of the effect of asymmetric geometry on residual stress distribution. *Journal of Materials Processing Technology*, 2008, 207(1): 211-221.
[31] M Erdogan, S Tekeli. The effect of martensite particle size on tensile fracture of surface-carburised AISI 8620 steel with dual phase core microstructure. *Material & Design*, 2002, 23(7): 597-604.
[32] W Wang. *Calculation on heat transfer coefficient of several typical steels in different quenchants*. Dalian: Dalian University of Technology, 2007. (in Chinese)